

# PORE-SCALE SIMULATION OF KHZ-GHZ ELECTROMAGNETIC DISPERSION OF ROCKS: EFFECTS OF ROCK MORPHOLOGY, PORE CONNECTIVITY, AND ELECTRICAL DOUBLE LAYERS

Emmanuel Toumelin, Chevron, and Carlos Torres-Verdín, the University of Texas at Austin

Copyright 2009, held jointly by the Society of Petrophysicists and Well Log Analysts (SPWLA) and the submitting authors.

This paper was prepared for presentation at the SPWLA 50<sup>th</sup> Annual Logging Symposium held in The Woodlands, Texas, United States, June 21-24, 2009.

## ABSTRACT

Increasing importance is being given to rock dielectric properties as multi-frequency electromagnetic (EM) logging tools continue to be developed in frequency ranges spanning kHz, MHz and even GHz. Applications are varied, from estimating hydrocarbon saturation, carbonates morphology, or rock wettability, to shale properties. Almost 30 years after pioneering studies on EM dispersion of saturated rocks, the problem remains to simultaneously integrate information on lithology, rock morphology, fluid distributions, and clay effects over the entire kHz-GHz range. This paper summarizes recent developments with a general pore-scale numerical framework for the wide-band simulation of conductivity and dielectric dispersion using two-dimensional (2D) digital rock models that include explicit pore and fluid distributions. The method rigorously honors Maxwell's equations and Kramers-Kronig's causal relations, and is validated with existing dielectric mixing laws. Simulation results emphasize the averaging effect of mixing laws and the need for numerical quantitative models. A sensitivity study confirms the importance of pore connectivity, a property neglected by effective medium theories. The simulation framework also provides microscopic justification and indicates possible limitations of dielectric measurements concerning their sensitivity to hydrocarbon saturation, wettability, and clay double-layers. Interpreting petrophysical properties from dielectric rock dispersions requires acquisition of multiple wide-band measurements, especially between 100 kHz and 10 MHz.

## INTRODUCTION

Judging from the abundance of recent SPWLA and SPE publications on the subject, it appears as though the study of rock dielectric effects in well-logging and petrophysics is undergoing a renaissance. Beginning as far back as the early 1980s, studies considered analytical models of EM dispersion (i.e., frequency

dependence). However, the outcome of those studies was not judged as commercially interesting by the oil industry. The only tools based on dielectric physics operated in the GHz range, above the dispersion frequency range, where the signal is consistently sensitive to shallow water-filled porosity almost regardless of salinity. At the same time, measurements were so shallow sensing and borehole effects so large that these tools only survived in niche applications, such as the assessment of residual oil saturation in low-salinity reservoirs.

In the early 2000s, development of LWD propagation tools in the MHz range prompted the study of dielectric effects to accurately process formation resistivity values to be compatible with kHz-range wireline logs and standard resistivity laboratory measurements. Most recently, Pathfinder published a series of papers on the topic (Haugland 2005; Haugland et al. 2006), exploring the possibility of interpreting fluid saturation from the frequency dispersion of LWD resistivity measurements (Illfelder et al. 2008). Simultaneously, Schlumberger published a series of papers not only about dielectric effects on LWD resistivity acquisition and inversion (Anderson et al. 2007), but also on dielectric effects arising in the kHz induction range (Anderson et al. 2006) as well as potential applications of dielectric dispersion in unconventional lithologies (volcanic, Altman et al. 2008; gas shales, Anderson et al. 2008). These papers describe the most recent developments on EM dispersion phenomena from a well-logging perspective. Core analysis also emphasized the potential of sub-MHz measurements to assess wettability (Garrouch 2001) and cation-exchange capacity (Garrouch 2008). Bona et al. (2001) suggested the comparison of conductivity measurements at different frequencies (including >20 MHz) to estimate rock wettability.

The GHz range so far has been exclusively used for calculations of shallow fluid saturation. This frequency range also became of interest among well-log analysts given its sensitivity to other petrophysical properties (Seleznev et al. 2004, 2006). As a result, Schlumberger is currently testing a new EM tool that operates in the 20 MHz – 1 GHz range (Hizem et al. 2008), which complements the frequencies of LWD propagation and wireline induction measurements for broadband

acquisition. Simultaneously, Clennell et al. (2006) remind us of the potential of wide-band EM measurements for shale characterization using the entire Hz-GHz range.

In the wake of this wave of new EM technology, it seems appropriate to recapitulate a recent numerical modeling approach that integrates a combination of petrophysical properties affecting the wide-band dispersion of EM measurements into *one model for the entire kHz-GHz range*. The principles of the work that is being summarized in this paper were first presented in a SCA conference paper (Toumelin et al. 2005), and then rigorously established for rock morphology effects by Toumelin and Torres-Verdín (2007). Subsequently, the numerical framework was extended to include clay double layers and wettability effects by Toumelin et al. (2008). The objective of this paper is to synthesize the approach and its main results, with a focus on establishing practical rules and guidelines for using wide-band EM dispersion phenomena in well-log interpretation.

### ROCK MORPHOLOGY VS ELECTRO-CHEMICAL DOUBLE LAYERS

Let us first review the reasons that justify numerical modeling of wide-band EM measurements. First, for nearly three decades it has been acknowledged that two main phenomena affect the EM dispersion of saturated rocks (Sen and Chew 1983): rock morphology and clay double-layers. Even though each phenomenon has been analytically quantified under ideal conditions (ideal grain or pore ellipsoids, finite-dilute limit, grain contact surface  $\ll$  rock/brine surface area, single non-amalgamate clay particles, etc.), the actual geometrical configuration and resulting EM coupling between scatterers have not been honored in a rigorous manner. More recent analytical methods exist that reflect a combination of morphology and electrochemical double-layer effects by way of percolation thresholds, power-laws, or fractal approaches. However, these approaches make parametric assumptions that are virtually impossible to verify in practice. Extensive review of such analytical models can be found in Toumelin et al. (2007, 2008). Prior to that, laboratory measurements (e.g. Bona et al. 1998; Myers 1991, 1996) also confirmed that the superposition of geometrical effects and clay double-layer effects explain the wide-band EM dispersions measured on saturated rock samples, except that the parameters used to fit the measured dispersions could not be directly related to petrophysical properties. The method described in this paper postulates realistic petrophysical properties and estimates corresponding EM dispersions.

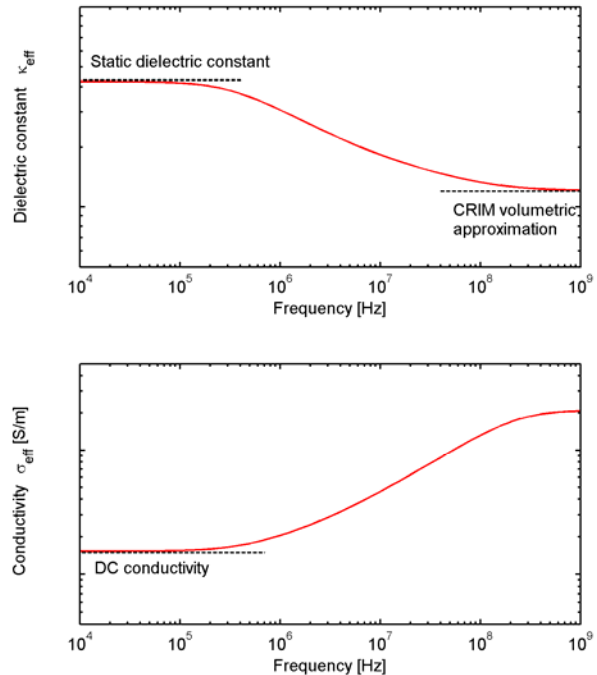
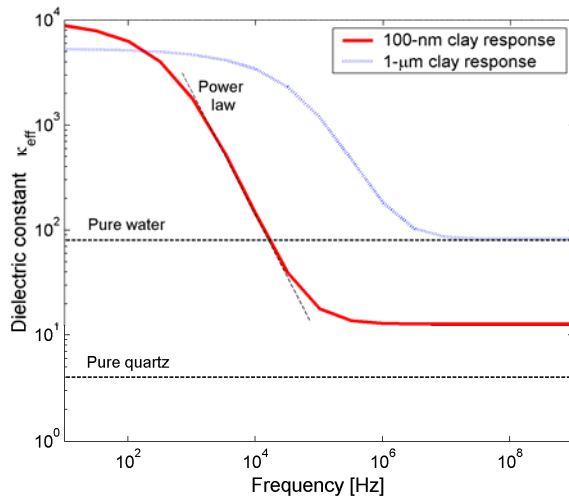


Fig. 1: Example of typical Maxwell-Wagner dispersion of dielectric constant and conductivity.

**Rock morphology effects.** Depending on the eccentricity of assumed ellipsoidal rock inclusions in a brine background (or brine-filled pore inclusions in a rock background), electric charges accumulate at the interface between brine and rock (or oil). Between these charged surfaces, brine polarizes in the form of a macroscopic dipole, which gives rise to frequency-dependent macroscopic polarization also known as Maxwell-Wagner effect. At low frequencies, macroscopic dipoles reach equilibrium before the incident field has notably changed, giving rise to polarization build-up. When frequency increases, the orientation of macroscopic dipoles cannot follow the applied field due to the viscosity of the fluid, thereby resulting in energy dissipation, increased electrical conductivity, and reduced dielectric permittivity. As depicted in Fig. 1, the resulting conductivities and dielectric permittivities take the shape of sigmoid functions of frequency. Dielectric constant is defined as the effective dielectric permittivity or the ratio of measured dielectric permittivity to vacuum permittivity,  $\epsilon_0$ . The low-frequency asymptote of the conductivity sigmoid is the DC conductivity measured on a rock sample with a traditional 2- or 4-pole resistivity electrode configuration, and is usually assimilated to Archie's equations to determine resistivity index; the high-frequency dielectric constant is usually assimilated

to the CRIM (complex refractive index) method to determine water-filled porosity.

**Electrochemical double-layer (EDL) effects.** Regardless of their approaches, the different EDL analytical models predict a strong enhancement of the dielectric constant of hydrated clay particles at low frequency as a function of clay size and surface charge. This behavior is explained by the reorganization of the cations present within the ionic double layer, in similar fashion to pore electrolyte building up (Maxwell-Wagner effect) at pore walls. In the present approach we conceive of an individual hydrated clay particle as a spherical unit described by the model of Fixman (1980) and previously used by Lima and Sharma (1992) in their generalized finite-dilution mixing law. Figure 2 shows an example of the electrical dispersions simulated with this latter model for a single hydrated clay particle (see Toumelin et al. 2008).



**Fig. 2:** Example of dispersion of dielectric constant of a clay particle using Fixman's model and assuming different sizes (100 nm and 1  $\mu\text{m}$ ), 0.1 S/m brine conductivity, and a surface charge equal to 11  $\mu\text{C}/\text{cm}^2$  (or  $6.9 \times 10^{17}$  ions/ $\text{m}^2$ ) compatible with measurements in smectites (Sonon and Thomson 2005). EDL yields extremely high values of dielectric constant at low values of frequency, well beyond water dielectric constant; truncation of the sigmoid dispersion below the kHz range would make it appear as a power-law relation, consistent with some experimental observations. Higher values of surface charge density (e.g., kaolinites as reported by Kanket et al. 2005) would make the dielectric enhancement even larger.

## NUMERICAL FRAMEWORK

The basic numerical framework consists of two sequential steps. First, the pore space is defined with an isotropic binary pore map (as used, for instance, in thin-section point counts), where the pore space is segregated from the solid rock matrix. Pore pixels can be further distributed between different fluid phases and matrix pixels can be assigned to represent minerals and clays. The resultant pore map is a spatial distribution of fluids, minerals, and clay particles limited by pixel resolution (Fig. 3). Each pixel is assigned electrical properties of the phase it represents, namely DC conductivity and high-frequency dielectric permittivity (or dielectric constant) remain unchanged for fluids and pure minerals over the kHz-GHz range. Hydrated clays themselves have frequency-dependent effective properties and are modeled using Fixman's approximation (Toumelin et al. 2008).

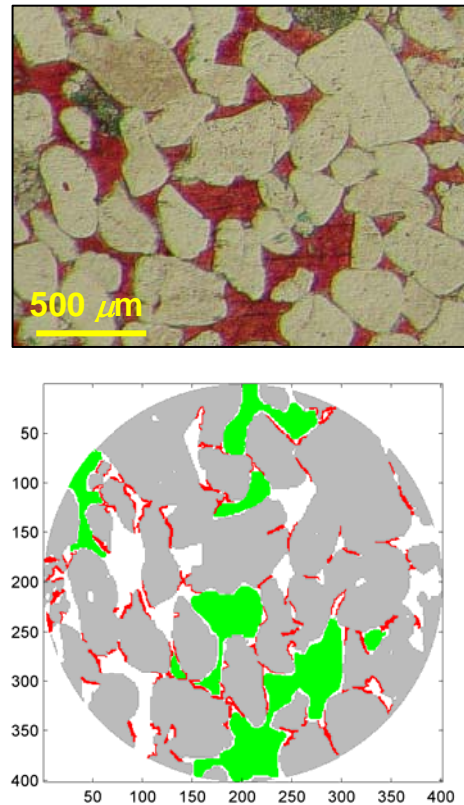


**Fig. 3:** Example of pore map adapted from a sandstone micrograph; gray represent grain matrix, red, pore coating clay cements, green, non-wetting hydrocarbon, and white, brine. Axes describe numbers of pixels. Pixel resolution is 5  $\mu\text{m}$ .

The second step consists of computing the frequency-domain internal electric fields of the pore map under EM excitation with a nominal incident plane wave. Calculations for the examples described below were performed with the method of moments. Figure 4 shows the internal electrical currents computed within a pore map by only including elliptical pores in the rock matrix, and with EM excitation in the form of perpendicular incident plane waves.

At a third step, a new inversion algorithm is used to compute the *effective* conductivity and dielectric permittivity of the pore map from the computed internal electric fields, as summarized below, at each frequency (Toumelin and Torres-Verdín 2007). Each pixel of the pore map is characterized by real-valued conductivity  $\sigma$ , dielectric constant  $\kappa$ , internal electric field  $\mathbf{E}$ , and complex conductivity, i.e.

$$\bar{\sigma}^* = \sigma - i\omega \varepsilon_0 \kappa, \quad (1)$$

where  $i$  is the complex imaginary unit,  $\omega = 2\pi f$ , and  $f$  is the frequency of EM excitation. A homogeneous medium with the same size and disc shape as the pore map is defined with arbitrary values of conductivity  $\sigma_h$ , dielectric constant  $\kappa_h$ , and complex conductivity

$\bar{\sigma}_h^* = \sigma_h - i\omega \varepsilon_0 \kappa_h$ . The corresponding internal electric field under the same plane wave incidence as that of the pore map is denoted by  $\mathbf{E}_h$ , and is computed analytically (plane wave scattered by a disc). The homogeneous disc is considered electrically equivalent to the pore map when it minimizes the cost function

$$\Psi = \left\| \bar{\sigma}^* \mathbf{E} - \bar{\sigma}_h^* \mathbf{E}_h \right\|_{L_2} + \left| \bar{\sigma}_b^* \right| \times \left\| \mathbf{E} - \mathbf{E}_h \right\|_{L_2}, \quad (2)$$

where the  $L_2$  norm is the mean-square average over all pixels of the pore map, and  $\left| \bar{\sigma}_b^* \right|$  is the norm of the complex conductivity of the lossy brine background.

We note that the proportion between the size of the geometrical features and the size of the model (in pixels) affects the quality of inversion results. If the pore map is anisotropic, i.e., if its effective properties substantially vary with the angle of incidence of the plane wave, then an anisotropic formulation of the homogeneous disc must be used in the analysis. All the results reported in this paper assume isotropic rock models.

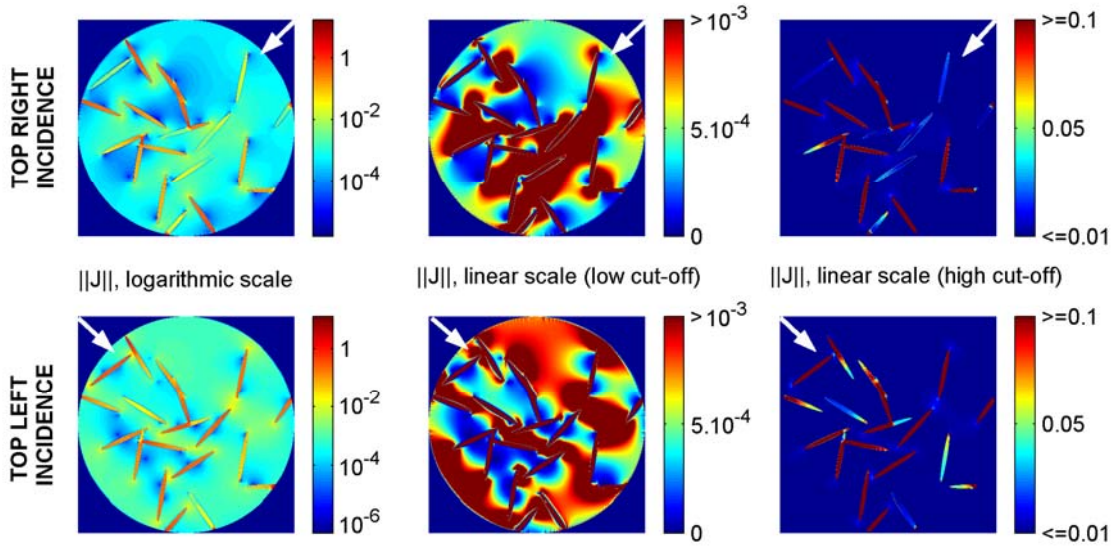


**Fig. 4:** Example of internal electrical currents calculated for a pore map that includes elliptical brine inclusions embedded in disc-shape rock matrix. Arrows represent the two simulated angles of plane wave incidence. The color scale describes the amplitude of the internal complex electric currents,  $\mathbf{J}$ , at 100 MHz on a pixel basis. Different scales emphasize the spatial distribution of electrical currents, both in the rock matrix and in the brine-filled pores (after Toumelin et al. 2008)

## VALIDATION OF THE SIMULATION MODEL

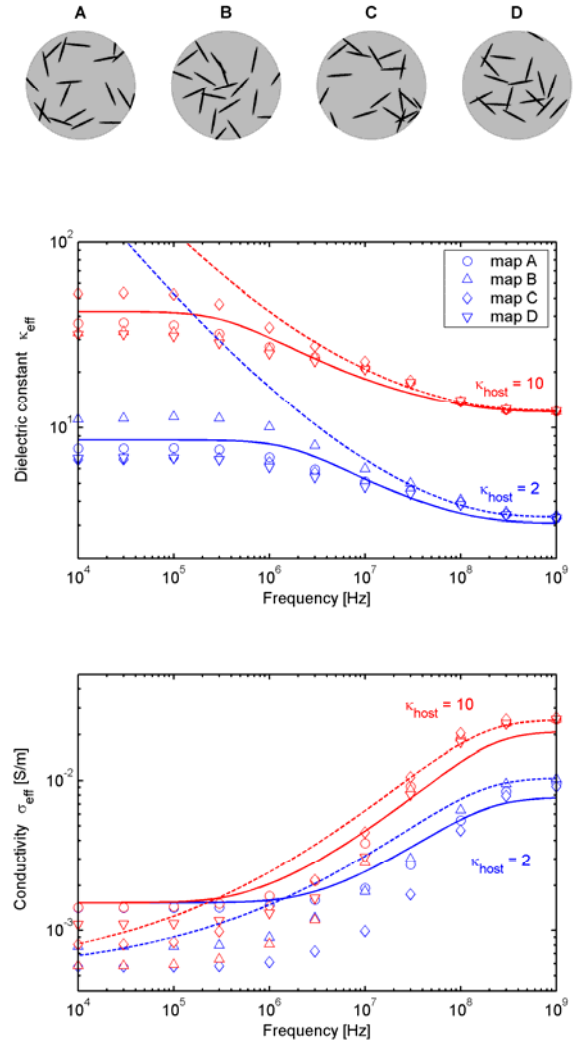
The numerical approach described in this paper is believed to yield effective electrical properties with superior accuracy than effective-medium theories because of the following three reasons:

- (1) Electric/magnetic duality of Maxwell's equations is explicitly enforced by the resolution of internal electric fields within the pore map and by the constraint imposed by Eq. (1) on inverted effective properties.
- (2) Kramers-Kronig's causal relations between effective conductivity and dielectric constant are verified on the simulation range (see below).
- (3) Inversion accuracy was verified on the entire kHz-GHz frequency range for values of DC conductivity from 0.001 S/m to 0.1 S/m, and values of dielectric constant from 20 to 2000 (Toumelin and Torres-Verdín 2007).

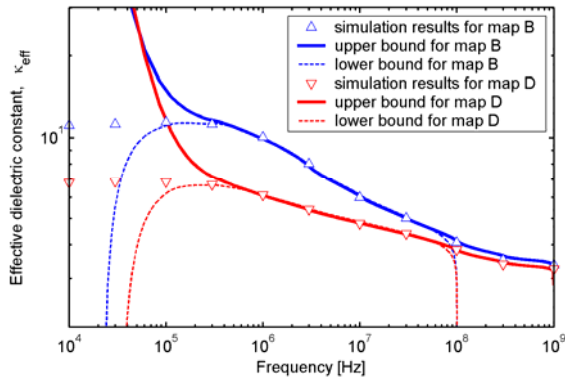
Figure 5 shows the dispersions simulated for a set of pore maps A to D assuming upper and lower bounds of rock dielectric constant (respectively, 2 and 10) compared to Mendelson and Cohen's Effective Medium Approximation (EMA – see Kenyon 1984). All pore maps exhibit the same porosity (8%) and the same ellipse aspect ratio (12). A conclusion from these results is that the mixing law averages the results from individual simulations. CRIM results are also compared and agree very well when predicting effective dielectric constant and conductivity above 100 MHz, but substantially diverge when predicting dielectric effects below that frequency range.

Figure 6 illustrates the compatibility of our simulation results with Kramers-Kronig's relations (Landau and Lifschitz 1960). These relationships establish a causality link between conductivity and dielectric constant, so that the dispersion exhibited by one of the two variables can be computed from the dispersion of the other variable over an infinite frequency range. Here, conductivity is numerically modeled on the truncated 10 kHz – 1 GHz frequency range and the corresponding Kramer-Kronig predictions yield the upper and lower bounds shown in Fig. 6. Between 400 kHz and 80 MHz, the simulated values of dielectric constant agree exactly with Kramers-Kronig predictions. Below 400 kHz and above 80 MHz the bounds diverge because of the absence of conduction data below 10 kHz and above 1 GHz, respectively. In those ranges, simulation results remain very stable and satisfy the range of uncertainty allowed by Kramers-Kronig's relation.

Finally, Fig. 7 shows that sensitivity to brine salinity is preserved by the simulation model.



**Fig. 5:** Example of pore maps with random distributions of similar brine elliptical pores, and computation results of their effective conductivity and dielectric constant at different frequencies. Dispersions were computed on the entire 10 kHz – 1 GHz range assuming rock dielectric constants equal to 2 (results in blue) or 10 (in red). Continuous lines identify results obtained with the EMA model for a 2D distribution of ellipses. Dashed lines identify results obtained with the CRIM model (after Toumelin and Torres-Verdín 2007).



**Fig. 6:** *Kramers-Kronig relations determine envelopes of possible values for  $\kappa_{eff}$  for each computed value of  $\sigma_{eff}$ , which are compared to values of  $\kappa_{eff}$  numerically simulated in Fig. 5.*

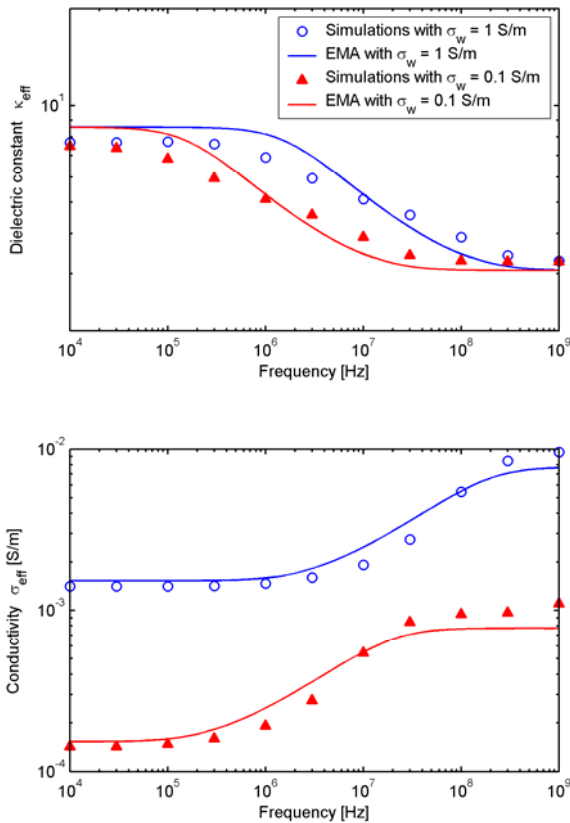


**Fig. 7:** *Comparison of electrical dispersions simulated for map A to those modeled with EMA, for two values of brine salinity.*

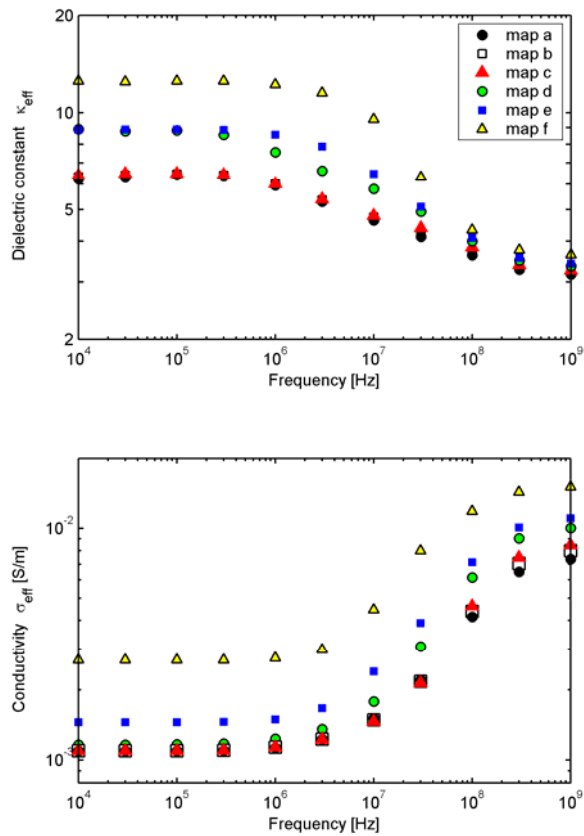
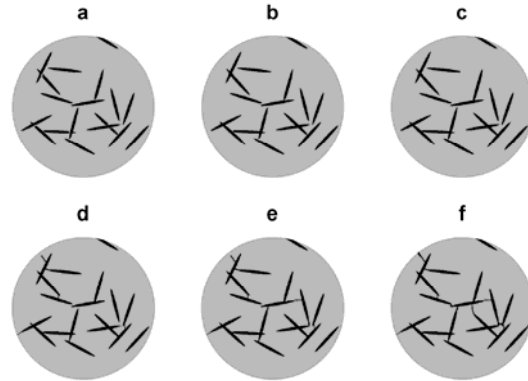


**Fig. 8:** *Pore maps modified from Map D of Fig. 4 with increasing degrees of connectivity between pores, and corresponding simulated dispersions of effective dielectric constant and conductivity.*

### PORE MORPHOLOGY VS CONNECTIVITY: THE MISSING LINK?

Mixing laws usually neglect communication between the pores or grains whose shape causes Maxwell-Wagner EM dispersion. We performed a sensitivity analysis to appraise communication effects based on the random distribution of elliptical pores of map D in Fig. 5, renamed map C in Fig. 8. First, a few water pixels were progressively removed from the map (thereby reducing pore connectivity while minimally affecting porosity), yielding maps B and A. Water pixels were also progressively added to map C to enable increasing pore connectivity at almost constant porosity, thereby yielding maps D, E, and F.

Figure 8 shows the electrical dispersion of effective conductivity and dielectric constant simulated for maps A to F. Effective properties of maps A-C are essentially identical, but they diverge as pore connectivity increases: conductivity overall increases several folds (percolation across the pore map is reached in map F). At the same time, the low-frequency dielectric constant increases as connected pores form pore clusters of variable aspect ratios. Consequently, pore connectivity does play a role in the dielectric dispersion of saturated rocks. Given the dimensional limitation of the model, there is no doubt that simulations performed with larger, three-dimensional (3D) rock models would shed more light to the relationship between pore morphology, connectivity, and EM dispersion. Establishing a method to diagnose and quantify connectivity of secondary porosity and microcracks from measurements of dielectric dispersion could be valuable in the petrophysical appraisal of certain rock formations.

### SATURATION EFFECTS

Partial water saturation can also be simulated with appropriate descriptions of pore-scale fluid distribution. Figure 9 describes a simple attempt to incrementally change fluid saturation in a realistic manner within the pore space of Figure 3 – as if the pore map were a slice through a 3D rock being desaturated. Starting from an irreducible-water state, water saturation increases and oil is left behind in the form of wetting and lenticular films. The pixel geometry reflects oil-wet conditions but it would vary minimally in water-wet conditions where no clays are present and where grain pixels could be substituted with oil pixels. Simulation results show a clear gradation of the spectrum of dielectric constant with saturation. In the GHz range, all Maxwell-Wagner

morphology effects dissipate regardless of brine salinity. This observation validates the use of CRIM-like residual oil saturation estimations within that frequency range.

In the MHz range, dispersion due to rock morphology is important whereby water saturation could be estimated from measured values of dielectric constant. This observation confirms the LWD measurements reported by Illfelder et al. (2008). Taking one step further, the same observation suggests that one could characterize the typical dielectric dispersion of a given formation at specific values of porosity and salinity through laboratory measurement of fully water-saturated samples or with log measurements acquired across a wet zone. Thereafter, the discrepancy between that reference dispersion and the measured dielectric dispersion (using at least a few frequency measurements) could be interpreted as a function of hydrocarbon saturation. From a conceptual viewpoint, inference of saturation from dielectric dispersion in the MHz range would have the advantage of being measured deeper than in the GHz range, except that it would remain sensitive to water salinity.

### EDL AND WETTABILITY

Our model assumes that the clay double layer is hydrated in water-wet conditions, and that clay polarization similar to that shown in Fig. 2 applies to the hydrated-clay pixels. Figure 10 shows a model for the desaturation of the pore map used previously which includes clay coatings in water-wet conditions along with the corresponding dielectric simulation results. Previous conclusions (considering absence of clay EDLs) remain valid, except that in the present situation pore morphology, hydrocarbon distribution, and hydrated clay double layers interact in a non-distinctive manner. Situations like this require explicit pore-scale modeling with coupling (in the EM sense) of all the microscopic features present for proper interpretation of dielectric dispersion.

The above simulated dielectric-dispersion signatures strongly resemble those measured by Bona et al. (1998) in Fig 11, which confirms the ability of the pore-scale framework to quantitatively predict dielectric dispersions and understand the underlying petrophysical properties. There is no doubt that such an approach would be useful to explain substantial dielectric effects observed in complex lithologies such as shales, where the breakdown between clay and hydrocarbon effects on dielectric dispersion is critical (Clennell et al. 2006; Anderson et al. 2008).

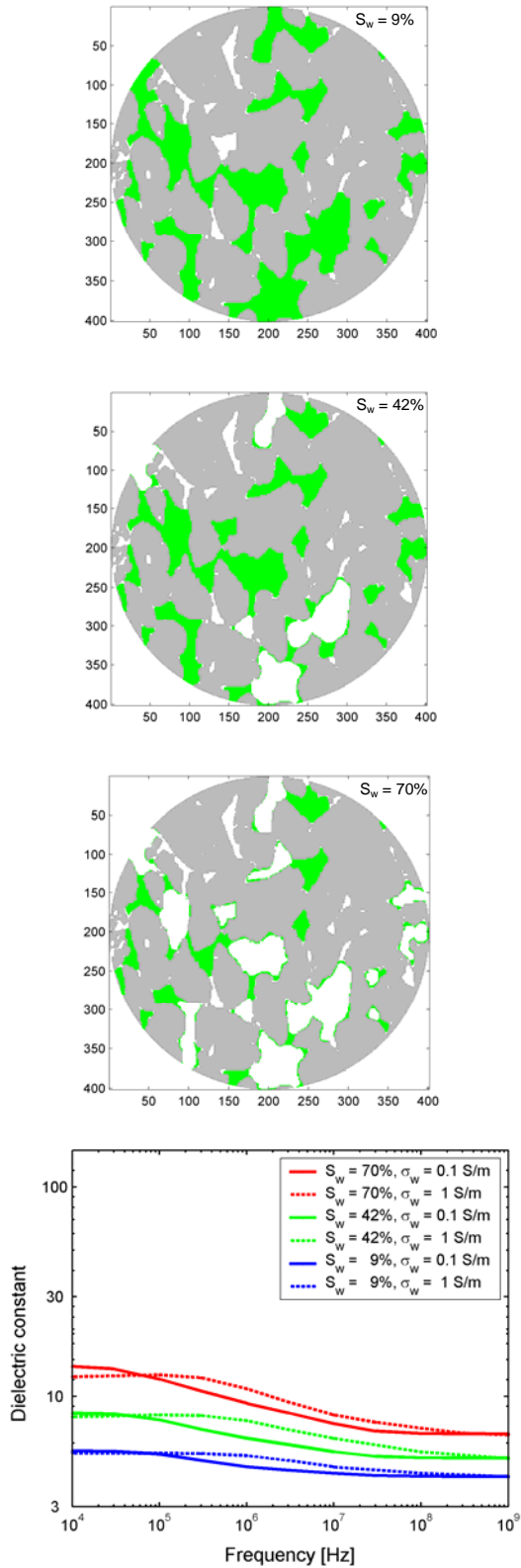


**Fig. 9:** Geometrical pixel representation of a simple rock desaturation model in oil-wet conditions, and corresponding simulation results of wide-band dielectric constant.

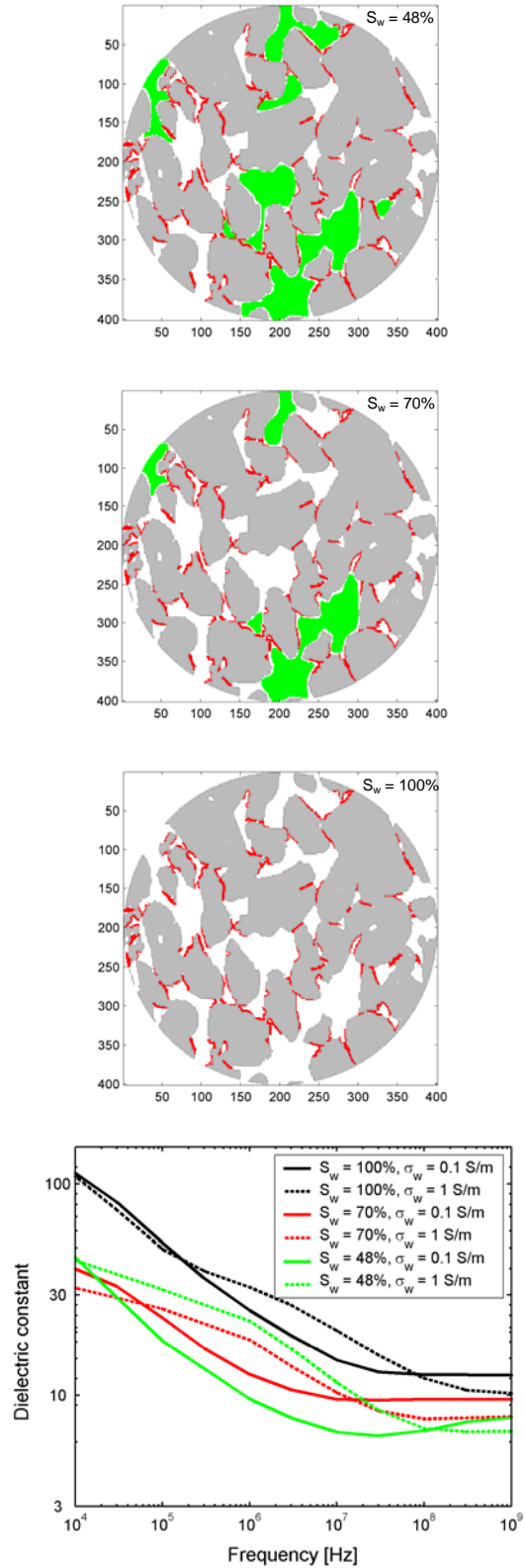


**Fig. 10:** Geometrical pixel representation of a simple rock saturation model in water-wet conditions, and corresponding simulation results of wide-band dielectric constant.

We remark that even for the most robust application of dielectric logging, i.e., saturation calculations at 1 GHz, differences persist between dielectric constant values computed at 1 GHz in Figs. 9 and 10, due to slight differences in pixel geometry (at similar saturation) and to clay effects remaining at that frequency. Bona et al.'s measurements show a similar behavior, whereby dispersions of dielectric constant do not necessarily converge to the same asymptotic value around 1 GHz, for the same value of water saturation, when rock wettability changes. This observation therefore suggests a possible wettability dependence of CRIM-like saturation calculations in the GHz range, which would be worth verifying with different EDL models, clay characteristics, clay amounts, and actual 3D modeling.

## CONCLUSIONS

This paper summarized a new pore-scale model to numerically simulate and microscopically justify wide-band EM dispersions of saturated rocks in the kHz to GHz range. The model is superior to existing effective-medium theories in its predictions of rock dielectric dispersion within that frequency range. Calculations performed with the new pore-scale model agree well with observed dielectric dispersions in well logging and core analysis across wide frequency ranges. Specifically, the model reproduced dielectric effects in the kHz range not previously explained for non-conventional lithologies and/or rock wettability states. Clay effects dominate dielectric dispersion in that frequency range, whereas geometric (Maxwell-Wagner) effects may become equally important to explain dielectric measurements acquired in shales and gas shales.

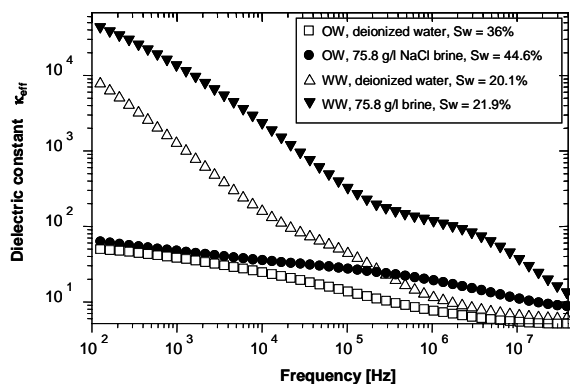


**Fig. 11:** Dielectric dispersions measured by Bona et al. (1998) on one sandstone rock sample treated to be both oil-wet (OW) and water-wet (WW), for different values of brine salinities and water saturation,  $S_w$ .

To a lower extent, the ability to measure dielectric constant in the kHz-MHz range using wireline or LWD tools could enable a viable measurement of wettability, as indicated by earlier core analysis. The range between 100 kHz and 10 MHz, in particular, is the richest in information, but is also most sensitive to several combined factors including pore morphology, connectivity, hydrated clay effects, salinity, and hydrocarbon saturation. Accounting for the individual contributions of these factors on dielectric dispersion will be necessary to gain petrophysical value from EM dispersion measurements. The same observation suggests combined interpretation of dielectric dispersion with other well-logging and core measurements. Standard saturation calculations assume knowledge of kHz-range resistivity, but the latter is not always compatible with LWD resistivity measured in the MHz range. In these cases it will be necessary to acquire measurements at several frequencies in order to assess the amplitude of the dispersions and estimate the low-frequency resistivity asymptote. Our numerical sensitivity study also confirmed the importance of pore connectivity, a property neglected by dielectric mixing laws which are commonly concerned only with Maxwell-Wagner effects.

Finally, the GHz range provides salinity-independent information on porosity and saturation. Simulation and laboratory results, however, suggest that wettability changes may affect the accuracy of such saturation calculations. Extending the numerical approach described in this paper to three dimensions is a promising and necessary development for quantitative interpretation of wide-band EM measurements and for validating new geometrical mixing laws.

## NOMENCLATURE

CRIM	Complex Refractive Index Method
EM	electromagnetic
EMA	Effective-Medium Approximation
$f$	frequency, (Hz)
$\mathbf{E}$	pixel internal electric field, (norm in V)
$\mathbf{E}_h$	homogeneous-medium internal electric field, (norm in V)
$\mathbf{J}$	pixel internal electrical current density
$S_w$	water saturation, (decimal fraction)
$\epsilon_0$	vacuum permittivity, ( $8.854 \times 10^{-12}$ Farad/m)
$\kappa$	pixel dielectric constant, (dimensionless)
$\kappa_{eff}$	effective dielectric constant, (dimensionless)
$\kappa_h$	homogeneous-medium dielectric constant, (dimensionless)
$\sigma$	pixel real conductivity, (S/m)
$\sigma_h$	homogeneous-medium real conductivity,

	(S/m)	
$\sigma_w$	water conductivity, (S/m)	
$\sigma_{eff}$	effective saturated rock conductivity, (S/m)	
$\bar{\sigma}^*$	pixel complex conductivity, (S/m)	
$\bar{\sigma}_b^*$	background complex conductivity	
$\bar{\sigma}_h^*$	homogeneous-medium complex conductivity	
$\omega$	radian frequency, (rad/s)	
$\Psi$	cost function for the inversion of the homogeneous-medium properties	

## ACKNOWLEDGEMENTS

The work described in this paper was funded by The University of Texas at Austin Research Consortium on Formation Evaluation, jointly sponsored by Anadarko, Aramco, Baker-Hughes, BG, BHP Billiton, BP, Chevron, ConocoPhillips, ENI, ExxonMobil, Halliburton, Hess, Marathon, Mexican Institute for Petroleum, Nexen, Petrobras, Schlumberger, StatoilHydro, TOTAL, and Weatherford.

## REFERENCES

- Altman, R., Anderson, B., Rasmus, J., and Lüling, M., 2008, Dielectric effects and resistivity dispersion on induction and propagation-resistivity logs in complex volcanic lithologies, a case study: Paper JJJJ, SPWLA annual logging symposium, Edinburgh, Scotland, May 25-28.
- Anderson, B., Barber, T., and Lüling, M., 2006, Observations of large dielectric effects on induction logs, or can source rocks be detected with induction measurements: Paper OOO, SPWLA Annual Logging Symposium, Veracruz, Mexico, Jun 4-7.
- Anderson, B., Barber, T., Lüling, M., Rasmus, J., Sen, P., Tabanou, J., and Haugland, M., 2007, Observations of large dielectric effects on LWD propagation-resistivity logs: Paper BB, SPWLA Annual Logging Symposium, Austin, Texas, Jun 3-6.
- Anderson, B., Barber, T., Lüling, M., Sen, P., Taherian, R., and Klein, J., 2008, Identifying potential gas-producing shales from large dielectric permittivities measured by induction quadrature signals: Paper HHHH, SPWLA Annual Logging Symposium, Edinburgh, Scotland, May 25-28.
- Bona, N., Rossi, E., Venturini, C., Cappaccioli, S., Lucchesi, M., and Rolla, P., 1998, Characterization of rock wettability through dielectric measurements: Revue de l'Institut Français du Pétrole, vol. 53 (6), 771-783.
- Bona, N., Rossi, E., Capaccioli, S., 2001, Electrical measurements in the 100 Hz to 10 GHz frequency range for efficient rock wettability determination: SPE Journal, vol. 6 (1), 80-88.
- Clennell, M.B., Dewhurst, D., and Raven, M., 2006, Shale petrophysics: electrical, dielectric and nuclear magnetic resonance studies of shales and clays: Paper KK, SPWLA Annual Logging Symposium, Veracruz, Mexico, Jun 4-7.
- Fixman, M., 1980, Charged macromolecule in external fields. I. The sphere: Journal of Chemical Physics, vol. 72 (9), 5177-5186.
- Garrouch, A., 2001, A comprehensive study of the relative dielectric permittivity in porous media: SPE paper 68779, SPE Western Regional Meeting, Bakersfield, California, Mar 26-30.
- Garrouch, A., 2008, An empirical model for estimating the rock lithology and the cation exchange capacity from dielectric permittivity data: SPE paper 113752, SPE Annual Technical Conference and Exhibition, Sep 21-24.
- Haugland, M., 2005, Frequency Dispersion Effects on LWD Propagation Resistivity Measurements: SPE paper 96596, SPE Annual Technical Conference and Exhibition, Dallas, Texas, Oct 9-12.
- Haugland, M., Badea, E.A., and Illfelder, H.M.J., 2006, LWD Propagation resistivity invasion processing based on dielectric-independent resistivities or on alternatively-parameterized resistivities: Paper TTT, SPWLA Annual Logging Symposium, Veracruz, Mexico, Jun 4-7.
- Hizem, M., Budan, H., Devillé, B., Faivre, O., Mossé, L., and Simon, M., 2008, Dielectric dispersion, a new wireline petrophysical measurement: SPE paper 116130, SPE Annual Technical Conference and Exhibition, Denver, Colorado, Sep 21-24.
- Illfelder, H.M.J., Badea, E.A., Boonen, P., and Liu, Z., 2008, Identification of formation fluids using the dielectric constant determined from LWD propagation measurements: Paper ZZZ, SPWLA Annual Logging Symposium, Edinburgh, Scotland, May 25-28.
- Kanket, W., Suddhiprakarn, A., Kheoruenromne, I., and Gilkes, R.J., 2005, Chemical and crystallographic

properties of Kaolin from ultisols in Thailand: *Clays and Clay Minerals*, vol. 53 (5), 478-489.

Kenyon, W.E., 1984, Texture effects on megahertz dielectric properties of calcite rock samples: *Journal of Applied Physics*, vol. 55, 3153–3159.

Landau, L.D., and E.M. Lifshitz, 1960, *Electrodynamics of continuous media*: Pergamon Press.

Lima, O.A.L., and M.M. Sharma, 1992, A general Maxwell-Wagner theory for membrane polarization in shaly sands: *Geophysics*, vol. 57, 431–440.

Myers, M.T., 1991, A saturation interpretation model for the dielectric constant of shaly sands: Paper 9118, Society of Core Analysts International Symposium, San Antonio, Texas, Aug 21-22.

Myers, M.T., 1996, A pore geometry dispersion model for the dispersion of the dielectric constant: Paper 9626, Society of Core Analysts International Symposium, Montpellier, France, Sep 8-10.

Seleznev, N., Boyd, A., Habashy, T., and Luthi, S.M., 2004, Dielectric mixing laws for fully and partially saturated carbonate rocks: Paper CCC, SPWLA Annual Logging Symposium, Noordwijk, the Netherlands, Jun 6-9.

Seleznev, N., Habashy, T., Boyd, A., and Hizem, M., 2006, Formation properties derived from a multi-frequency dielectric measurement: Paper VVV, SPWLA Annual Logging Symposium, Veracruz, Mexico, Jun 4-7.

Sen, P.N., and Chew, W.C., 1983, The frequency dependent dielectric and conductivity response of sedimentary rocks: *Journal of Microwave Power*, vol. 18 (1).

Sonon, L.S., and Thompson, M.L., 2005, Sorption of a nonionic polyoxyethylene lauryl ether surfactant by 2:1 layer silicates: *Clays and Clay Minerals*, vol. 53 (1), 45-54.

Toumelin, E., Torres-Verdín, C., and Bona, N., 2005, A new pore-scale framework for the simulation and interpretation of wide-band dielectric measurements: Paper 0521, Society of Core Analysts International Symposium, Toronto, Canada, Aug 21-25.

Toumelin, E., and Torres-Verdín, C., 2007, Two-dimensional pore-scale simulation of wide-band

electromagnetic dispersion in saturated rocks: *Geophysics*, vol. 72 (3), F97-F110.

Toumelin, E., Torres-Verdín, C., and Bona, N., 2008, Improving petrophysical interpretation with wide-band electromagnetic measurements: *SPE Journal*, vol. 13 (2), 205-215.

## ABOUT THE AUTHORS

**Emmanuel Toumelin** holds an engineering degree from the Ecole Centrale de Lille and a PhD in petroleum engineering from the University of Texas at Austin. His graduate research work focused on the pore-scale modeling of NMR and electromagnetic rock measurements. He has been a petrophysicist with Chevron North America Exploration and Production since 2006, and has worked on a variety of US Midcontinent and Alaska assets. He is on the editorial boards of *SPE Reservoir Evaluation and Engineering* and *SPE Journal*, and an associate editor for *Petrophysics*. He is a recipient of SPLWA's awards for best conference paper and best *Petrophysics* paper for fundamental pore-scale work on shaly-sand conductivity.

**Carlos Torres-Verdín** received a Ph.D. degree in Engineering Geoscience from the University of California, Berkeley, in 1991. During 1991–1997 he held the position of Research Scientist with Schlumberger-Doll Research. From 1997–1999, he was Reservoir Specialist and Technology Champion with YPF (Buenos Aires, Argentina). Since 1999, he has been with the Department of Petroleum and Geosystems Engineering of The University of Texas at Austin, where he currently holds the position of Zarrow Centennial Professor in Petroleum Engineering. He conducts research on borehole geophysics, formation evaluation, well logging, and integrated reservoir characterization, and is founder and director of The University of Texas at Austin's Joint Industry Research Consortium on Formation Evaluation. Torres-Verdín has served as Guest Editor for Radio Science, and is currently a member of the Editorial Board of the *Journal of Electromagnetic Waves and Applications*, and an associate editor for *Petrophysics* (SPWLA), the *SPE Journal*, and *Geophysics*. He is recipient of the 2003, 2004, 2006, and 2007 Best Paper Awards by *Petrophysics*, is recipient of the 2006 Best Presentation Award and of the 2007 Best Poster Award by the SPWLA, and is recipient of SPWLA's 2006 Distinguished Technical Achievement Award and SPE's 2008 Formation Evaluation Award.